Available online at www.sciencedirect.com

ScienceDirect

Ceramics International 40 (2014) 7761–7768

CERAMICS INTERNATIONAL

www.elsevier.com/locate/ceramint

Photochemical synthesis of $AZrO_{3-X}$ thin films (A = Ba, Ca and Sr) and their characterization

G. Cabello[a,*], L. Lillo[a], C. Caro[a], G.E. Buono-Core[b], B. Chornik[c], M. Flores[c], C. Carrasco[d], C.A. Rodriguez[d]

[a]Departamento de Ciencias Básicas, Facultad de Ciencias, Universidad del Bío-Bío, Chillán, Chile
[b]Instituto de Química, Pontificia Universidad Católica de Valparaíso, Valparaíso, Chile
[c]Deparamento de Física, Facultad de Ciencias Físicas y Matemáticas, Universidad de Chile, Santiago 8370415, Chile
[d]Departamento de Ingeniería de Materiales, Facultad de Ingeniería, Universidad de Concepción, Edmundo Larenas 270, Concepción, Chile

Received 27 November 2013; received in revised form 26 December 2013; accepted 27 December 2013
Available online 3 January 2014

Abstract

(Ba, Ca, Sr)ZrO_{3-X} thin films were prepared by a photochemical method using thin films of β-diketonate complexes as precursors. The photolysis of these films induces the fragmentation of the 2,2,6,6-tetramethyl-3,5-heptanedionate ligand and the partial reduction of metal ion together with volatile organic compounds as sub-products. When the metallic complexes are irradiated in air, the final product of the reaction are ternary metal oxides. The photoreactivity of these films was monitored by FT-IR spectroscopy by a period of 72 h, followed by post-annealing at 950 °C. X-ray photoelectron spectroscopy and X-ray diffraction techniques were used to analyze the chemical composition and the crystalline structure of the films obtained. The results indicate that Ba, Ca, Sr, Zr and O are present in the form of perovskita, preferably adopting an amorphous structure. The surface morphology examined by atomic force microscopy revealed a rough and irregular surface. The UV–vis measurements suggest a slight increase in the optical band gap values, which promote a reduction of the intermediary energy levels or defects.

Keywords: D. Perovskite; Photodeposition; Thin films; Ternary metal oxides

1. Introduction

The perovskite structure has the general formula ABO_3, where A and B are cations and O is an anion. The A and B cations can have a variety of charges and in the original perovskite mineral ($CaTiO_3$) the A cation is divalent and the B cation is tetravalent. Similar compounds that comply with this structure are: $AZrO_3$, $ASnO_3$, $AHfO_3$, where A = Ba(II), Ca (II), Sr(II) are just some examples. The perovskite has attracted considerable attention and constitutes one of the most important classes of mixed oxides [1]. These ceramic structures are the subject of extensive research due to their important physical characteristics, chemical stability and mechanical properties. However, it is now widely accepted that materials exhibit novel properties when their sizes decrease to nanometer scales, and the performance of materials depends largely on the synthesis procedure [2]. Different methods have been reported in the literature for the synthesis of $CaZrO_3$ and similar compounds. These structures were initially prepared by a conventional solid-state reaction between ZrO_2 and $CaCO_3$ or CaO at high temperatures (> 1200 °C). However the structures obtained by this method present several problems, such as high-processing temperatures, inhomogeneity and contamination by impurities with a non-uniform particle size distribution [3]. To minimize these problems, numerous methods have been employed to synthesize perovskites with the desired stoichiometry. These include sol–gel techniques [4,5], pulsed laser deposition [6,7], chemical solution deposition [8,9], chemical vapor deposition [10,11], among other methods. The photochemical synthesis of ceramic materials with UV light irradiation is different from other methodologies because it is highly selective. This selectivity occurs because the light absorption features of the reactants determine the reaction products. In this article, we report about the application of a photochemical method in the synthesis of $AZrO_3$ thin films

*Corresponding author. Tel.: +56 42 463096; fax: +56 42 463046.
E-mail address: gcabello@ubiobio.cl (G. Cabello).

0272-8842/$ - see front matter
http://dx.doi.org/10.1016/j.ceramint.2013.12.118

(where A=Ca, Ba and Sr). This method consists of the direct irradiation of a coordination complex with ultraviolet light on substrates which are not affected by the UV light. The development of this method requires that the precursor complexes form stable amorphous thin films upon spin coating onto a suitable substrate and that photolysis of these films result in the photoextrusion of the ligands leaving the inorganic products on the surface (Eq. (1)).

$$A(\beta-\text{diketonate})_2 + Zr(\beta-\text{diketonate})_4 + O_{2(g)} \xrightarrow{h\nu} AZrO_{3-X(\text{thin film})} + \text{sub}-\text{products} \quad (1)$$

Where: A = Ba, Ca, Sr. ß-diketone = 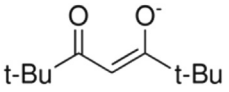

2. Experimental details

2.1. Preparation of amorphous thin films

The precursors Zr(IV), Ba(II), Ca(II) and Sr(II) 2,2,6,6-tetramethyl-3,5-heptanedionate (tmhd) complexes were purchased from Aldrich Chemical Company. The $Zr(tmhd)_4$ and $A(tmhd)_2$ complexes were mixed in a molar proportion of 1:1 in CH_2Cl_2 dissolution. The thin films were prepared by the following procedure: a silicon chip was placed on a spin coater and rotated at a speed of 600 rpm. A portion (0.5 ml) of a solution of the precursor complexes in CH_2Cl_2 was dispensed onto the silicon chip and allowed to spread. The motor was then stopped after 30 s and a thin film of the precursor remained on the chip. The quality of the films was examined by optical microscopy (500× magnification) and in some cases by SEM.

2.2. Photolysis of complexes as films on Si(100) surfaces

The substrates for deposition of films were quartz plates ($2 \times 2\ cm^2$) and p-type silicon(100) wafers ($1 \times 1\ cm^2$) obtained from Wafer World Inc., Florida, USA.

All photolysis experiments were done following the same procedure. The Fourier transform infrared (FT-IR) spectrum of the starting film was first obtained. The chip was then placed under a UV-lamp setup equipped with two 254 nm 6 W tubes, in air atmosphere. Progress of the reactions was monitored by determining the FT-IR spectra at different time intervals, following the decrease in the IR absorption of the complexes. After the FT-IR spectrum showed no evidence of the starting material, the chip was rinsed several times with dry acetone to remove any organic products remaining on the surface, prior to analysis. In order to obtain films of a specific thickness, successive layers of the precursors were deposited by spin-coating and irradiated as above. This process was repeated several times until the desired thickness was achieved. Post-annealing was carried out under a continuous flow of synthetic air at 950 °C for 2 h in a programmable Lindberg tube furnace.

2.3. Characterization of the thin films

The FT-IR spectra were obtained with 4 cm^{-1} resolution in a Perkin Elmer Series Spectrum Two FT-IR spectrophotometer. UV spectra were obtained with 1 nm resolution in a Perkin Elmer Model Lambda 25 UV–vis spectrophotometer. X-ray diffraction (XRD) patterns were obtained using a D8 Advance Bruker X-ray diffractometer, the X-ray source was Cu 40 kV/30 mA. X-ray photoelectron spectra (XPS) were recorded on an XPS-Auger Perkin Elmer electron spectrometer Model PHI 1257, which included an ultra high vacuum chamber, a hemispherical electron energy analyzer and an X-ray source providing unfiltered Kα radiation from its Al anode ($h\nu = 1486.6$ eV). The pressure of the main spectrometer chamber during data acquisition was maintained at ca 10^{-7} Pa. The binding energy (BE) scale was calibrated by using the peak of adventitious carbon, setting it to 284.6 eV. The accuracy of the BE scale was ±0.1 eV.

The surface morphology of the samples has been examined using atomic force microscopy (AFM) was performed in an AFM/STM Omicron Nanotechnology model SPM1 in contact mode. Film thickness was determined using a Leica DMLB optical microscope with a Michelson interference attachment.

3. Results and discussion

3.1. Evaluation of photo-reactivity of the precursor complexes

The photochemistry in solution of several transition metal 1,3-diketonates has been extensively studied [12,13]. It is known that these β-diketonate complexes absorb strongly at readily accessible parts of the UV spectrum (200–400 nm) and that irradiation of these complexes with UV light leads to the photo-reduction and the photo-fragmentation of these complexes. In some cases these photochemical processes were applied to the deposition of nano-particles and nanostructures films [14,15]. The photo-reactivity of zirconium β-diketonate complexes has previously been studied in our group [16]. The photochemical behavior of the Ba(II), Ca(II), and Sr(II) 2,2,6,6-tetramethyl-3,5-heptanedionate complexes has been investigated in dichloromethane solutions. Fig. 1 shows the electronic absorption spectra of these complexes in diluted solutions ($< 10^{-4}$ mol/L). They all exhibit a single band at 276 nm, attributable to ligand transition π–π*. The irradiation of dichloromethane solutions of the complexes at 254 nm causes spectral changes, consisting in a gradual decrease of the absorption bands at 276 nm after 230 min. Fig. 1 shows the UV profile of the photoreaction obtained by determining the UV spectra of samples taken in a range of 5–15 min intervals for the complexes. These results demonstrate that these β-diketonate complexes are highly photoreactive in solution when irradiated with 254 nm UV light.

In order to investigate the solid-sate photochemistry, films of the mixed-metal precursor complexes were deposited on Si wafers by spin-coating and irradiated under air atmosphere with a 254 nm UV source. The irradiation at 24, 48 and 72 h of these films under air atmosphere, led to a decrease of the

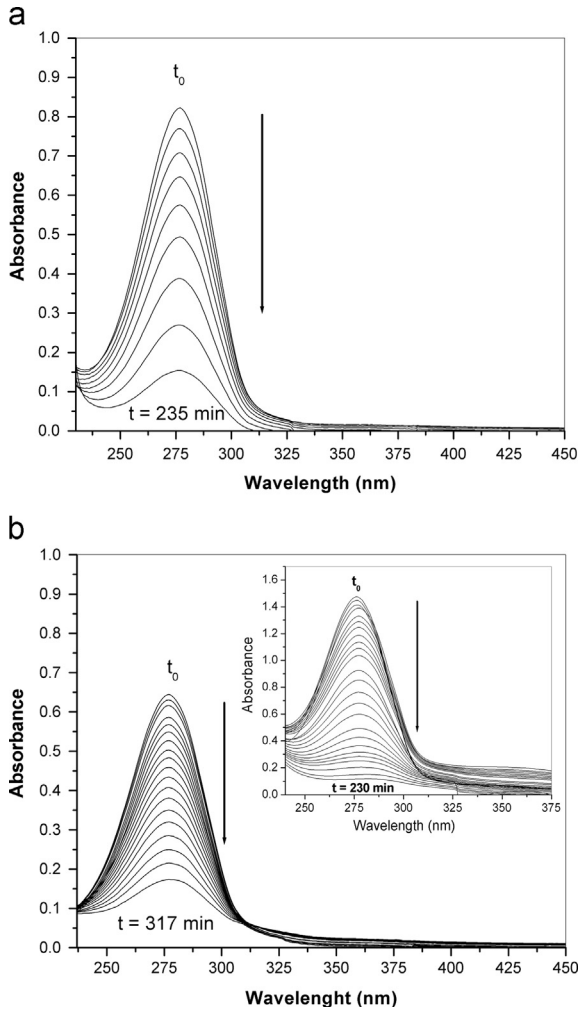

Fig. 1. Changes in the UV spectrum of a solution in CH_2Cl_2 of (a) $Ca(tmhd)_2$ complex (4.92×10^{-5} mol/L) upon 235 min irradiation and (b) $Ba(tmhd)_2$ complex (6.36×10^{-5} mol/L) upon 317 min irradiation. Inset: $Sr(tmhd)_2$ complex (4.31×10^{-4} mol/L) upon 230 min irradiation with 254 nm light.

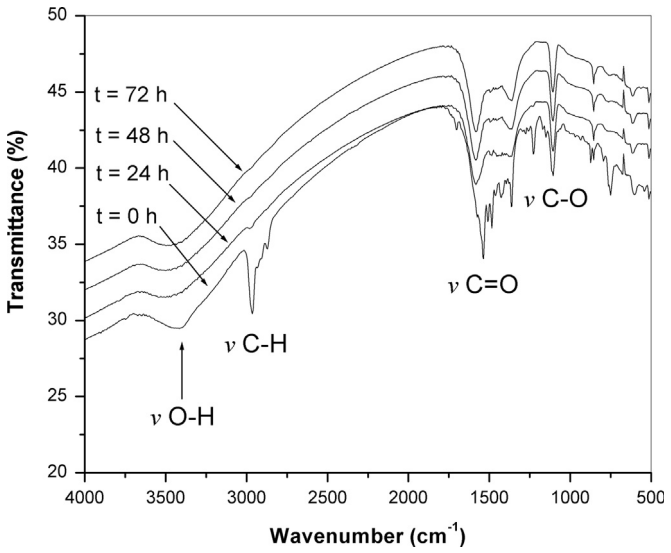

Fig. 2. Changes in the FT-IR spectra of films obtained upon 72 h irradiation with 254 nm light of $A(tmhd)_2$ and $Zr(tmhd)_4$ complexes, in a molar proportion of 1:1, where A = Ca(II), Ba(II), and Sr(II).

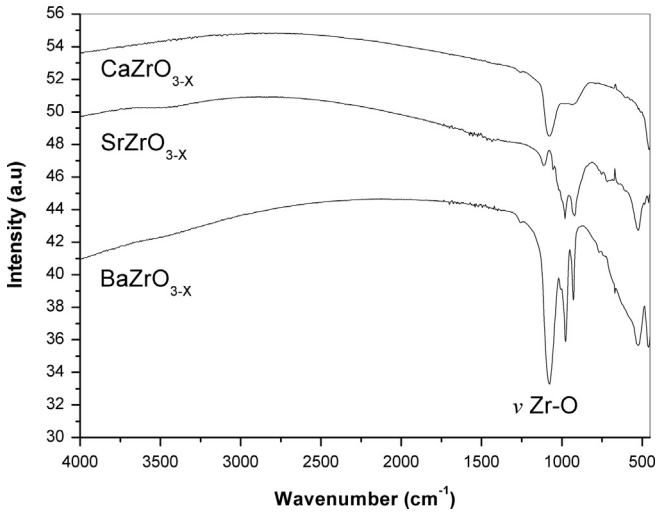

Fig. 3. FT-IR spectra for the films photodeposited and annealed at 950 °C for 2 h.

absorptions associated with the ligands, as shown by FT-IR monitoring of the reaction. At time zero (t_0) we see in Fig. 2 the vibration modes corresponding to β-diketonate complexes at 2970, 1570 and 1105 cm^{-1} attributed to C–H, C═O and C–O groups, respectively. All these peaks are characteristics of the precursor complexes, except the one at 3490 cm^{-1}, which is due to the presence of adsorbed moisture. At the end of the photolysis, after a 72 h irradiation period, minimum absorptions can be observed in the infrared spectrum. These absorptions correspond to sub-products, generated by fragmentations of the diketonate complexes on the surface, which are removed by washing with dry acetone. In Fig. 3 shows that the post-annealed films at 950 °C present no evidence of organic sub-products in the films, while the bands located between 1080 and 950 cm^{-1} can be attributed to the stretching vibrations of Zr–O and other bands located between 530 and 470 cm^{-1} corresponding to O–Zr–O stretching vibrations in the perovskite structure. These results agree with values reported by other authors [10,17,18].

3.2. Characterization of $AZrO_{3-X}$ thin films (where A=Ba, Ca or Sr)

3.2.1. XRD and XPS analysis

The crystalline structure of the films was analyzed by X-ray diffraction (XRD). Fig. 4 shows the XRD spectra taken after annealing the films at 950 °C for 2 h. Only the sample of barium zirconate shows peaks characteristic of a perovskite cubic structure at 30.2°, 43.2° and 53.6° which correspond to (1,1,0), (2,0,0) and (2,1,1) in agreement with JCPDS 6-0399 standard for cubic phase of $BaZrO_3$ [19]. Given the characteristics of our films it is possible that the thinner films contain a fraction of amorphous phase, which cannot be detected by X-ray diffraction. Thus, the photo-deposits may consist in a mixture of crystalline and amorphous fractions. Similar results

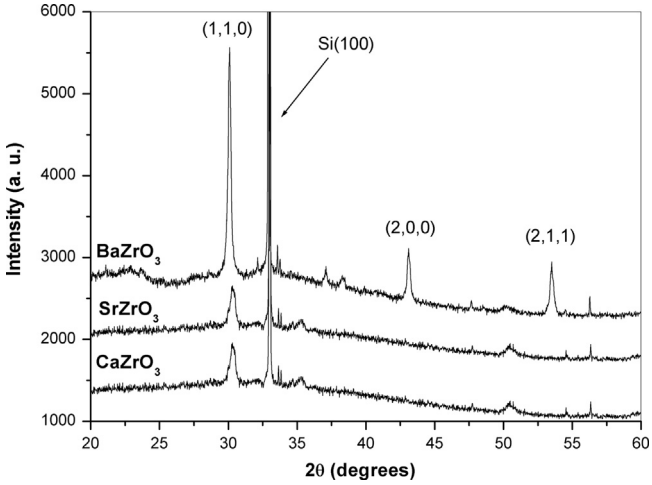

Fig. 4. XRD pattern of the photodeposited $AZrO_3$ films on Si(100) substrates annealed in air at 950 °C for 2 h.

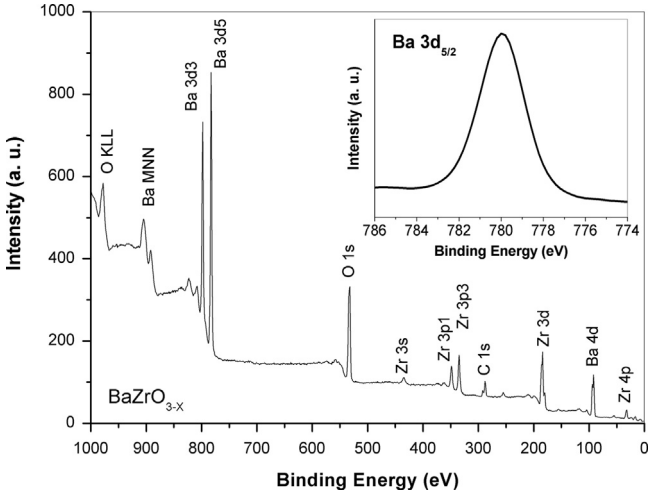

Fig. 5. XPS survey spectrum of $BaZrO_{3-X}$ thin film prepared by UV irradiation at 254 nm and annealed at 950 °C for 2 h. Inset figure: Ba $3d_{5/2}$ peak in the 774–786 eV region.

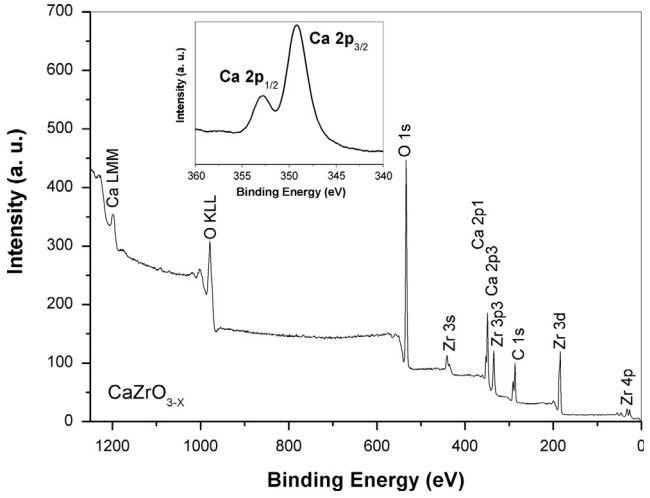

Fig. 6. XPS survey spectrum of $CaZrO_{3-X}$ thin film prepared by UV irradiation at 254 nm and annealed at 950 °C for 2 h. Inset figure: Ca 2p peaks in the 340–360 eV region.

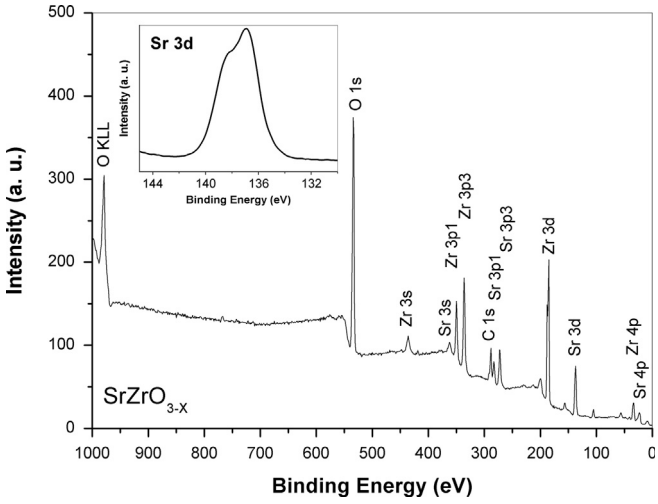

Fig. 7. XPS survey spectrum of $SrZrO_{3-X}$ thin film prepared by UV irradiation at 254 nm and annealed at 950 °C for 2 h. Inset figure: Sr 3d peaks in the 130–145 eV region.

have been reported in the synthesis of amorphous perovskites by modified sol–gel methods [20,21].

The chemical composition of the annealed thin films was determined by X-ray photoelectron spectroscopy (XPS). In Figs. 5–7 are shown the wide-scan XPS spectra of the $AZrO_{3-X}$ thin films. All the binding energies at various peaks were calibrated by the binding of C 1s (284.6 eV). For all these films, spectra show that O, Zr and C elements were present. The C 1s photoelectron peaks for the different samples appearing near 284.8 eV can be attributed to the organic residual from the precursors. Indeed, it has been documented [22,23] that the C 1s signal mainly shows three contributions at 288.9, 286.6 and 284.8 eV assigned to CO_3^{2-}, C–O and C–H/C–C species, respectively.

The XPS spectrum of the Zr 3d peak presents a doublet signal with energies at 182.2 eV ($3d_{5/2}$ level) and 184.6 eV ($3d_{3/2}$ level) with a spin–orbit distance (ΔE) between the two peaks of 2.4 eV. The peak positions and energy separations are in good agreement with data reported for Zr 3d binding energy values of other oxides with perovskite structures such as $BaZr_{0.05}Ti_{0.95}O_3$ [23] and $CaZrO_3$ [24].

The feature in the XPS spectrum of the O 1s peak is also a doublet structure, and each component peak in the spectrum was fitted to a Gaussian type distribution. The lower binding energy signal at 529.6 eV is associated to oxygen in the $AZrO_{3-X}$ lattice, as observed in other perovskite oxide compounds [25,26], and the high binding energy peak at 531.8 eV can be assigned to the hydroxyl groups or adsorbed oxygen species on the surface of films [27]. The binding energy values for different elements are listed in Table 1.

Fig. 5 shows the wide scan XPS spectrum of the $BaZrO_{3-X}$ thin films in which Ba 3d signals consist of two peaks

Table 1
Binding energies (± 0.1 eV) obtained by XPS analyses of $AZrO_{3-X}$ thin films.

ABO_3/signal	Ba $3d_{5/2}$	Ca $2p_{3/2}$	Ca $2p_{1/2}$	Sr $3d_{5/2}$	Sr $3d_{3/2}$	Zr $3d_{5/2}$	Zr $3d_{3/2}$	O 1s
$BaZrO_{3-X}$	780.1					181.4	183.8	529.6[a] 531.6[b]
$CaZrO_{3-X}$		347.3	350.9			182.3	184.6	529.9[a] 531.8[b]
$SrZrO_{3-X}$				133.6	135.3	182.2	184.6	529.3[a] 532.2[b]
Standard values[c]	779–781	346–347	348–350	132–133	134–135	181–182	183–185	529 – 530[a] 531 – 532[b]

[a]Attributed to lattice oxygen.
[b]Attributed to chemisorbed oxygen on the surface of film.
[c]Ref. [28].

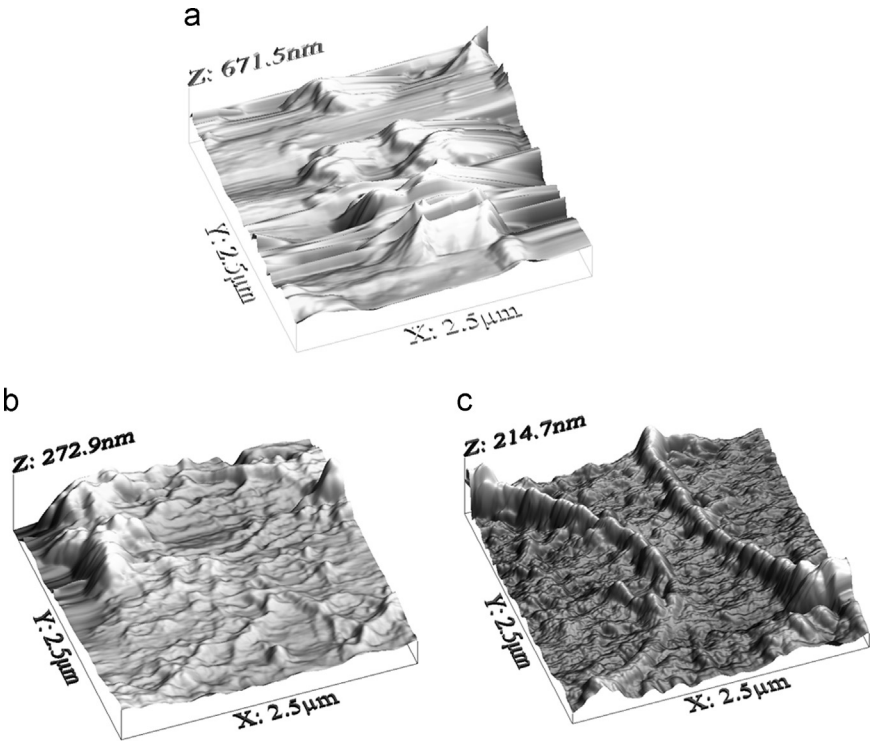

Fig. 8. AFM micrographs of annealed at 950 °C samples on Si(100), (a) $BaZrO_{3-X}$; (b) $CaZrO_{3-X}$; and (c) $SrZrO_{3-X}$ films.

identified as Ba $3d_{5/2}$ and Ba $3d_{3/2}$. The Ba $3d_{5/2}$ peak resolved in a single component at 780.1 eV (inset Fig. 5) is associated to Ba–O bonds [22,29].

Fig. 6 shows the wide scan XPS spectrum of $CaZrO_{3-X}$ thin films. It can be seen that the Ca 2p signal is a mixture of two overlapping peaks (inset Fig. 6). These are attributed to Ca $2p_{3/2}$ and Ca $2p_{1/2}$ at 347.3 and 350.9 eV respectively, with a binding energy (BE) separation of 3.6 eV. These results are in good agreement with BE values reported for other types of perovskite such as $CaSnO_3$ [29] and $CaTiO_3$ [30].

The XPS spectra for thin films of $SrZrO_{3-X}$ are shown in Fig. 7. The Sr 3d signal can be fitted to two main sub-peaks, one centered at 133.6 eV and the other at 135.3 eV. These signals have been attributed to photoemission peaks from Sr $3d_{5/2}$ and Sr $3d_{3/2}$, respectively. The energy separation between the Sr $3d_{5/2}$ and Sr $3d_{3/2}$ peaks were 1.7 eV. These measurements are consistent with those reported for strontium in the Sr^{2+} state present in $SrSnO_3$ [29] and $SrTiO_3$ [31]. However, a rigorous examination of the Sr 3d peak reveals other minor peaks which are very difficult to distinguish, but an appropriate fitting indicates other chemical states (Sr^0 and Sr^+) [28].

3.2.2. Morphology characteristics

Atomic force microscopy (AFM) was used to characterize the morphology of the annealed samples. Fig. 8 presents a series of topographic images from (a) $BaZrO_{3-X}$, (b) $CaZrO_{3-X}$ and (c) $SrZrO_{3-X}$ films. All these films have similar surface morphology, consisting a non-uniform surface which is characteristic for

an amorphous deposit, with a root-mean-square (RMS) roughness of (a) 40.1 ± 21.3; (b) 31.2 ± 13.1 and (c) 28.5 ± 12.5 nm, respectively. These values reflect the irregularity of the surfaces of the films obtained.

3.2.3. Optical properties

Fig. 9 shows the optical transmission spectra of the photo-deposited films on fused quartz, with a 250 ± 25 nm thickness. It can be seen from the UV–vis spectrum that the transmittance of films is close to 90% in the visible range for the $CaZrO_{3-X}$ and the $SrZrO_{3-X}$ films. A slight decrease in samples of $BaZrO_{3-X}$ films can be attributed to a greater thickness in the deposition obtained. A slight decrease of the transmittance below 250 nm is the absorption edge, which is related to the energy band gap of the materials [25]. A more accurate estimation of the band gap E_g can be obtained from the following relation (Eq. (2)).

$$(\alpha hv)^2 = \text{const}(hv - E_g) \quad (2)$$

where hv is the energy of incident photon, and α is the optical absorption coefficient, which can be estimated from the transmittance values using the relation (Eq. (3)).

$$T = A \exp(-\alpha d) \quad (3)$$

where d is the film thickness and A is a coefficient related to the refractivity, which is nearly equal to unity at the absorption edges [25].

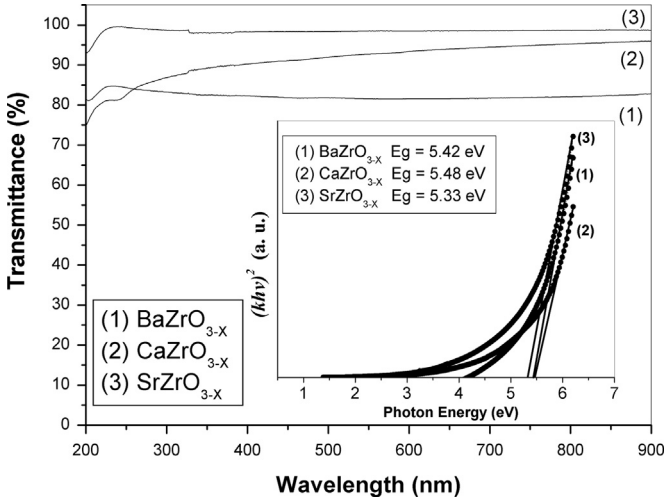

Fig. 9. Transmission spectra for the $AZrO_{3-X}$ thin films. Inset: square of absorption coefficient as a function of the photon energy.

In this case, the optical band gap was determined by extrapolating the linear portion of the curve or tail (see inset Fig. 9). The results of the optical band gap values of photo-deposited $AZrO_{3-X}$ are presented in Table 2. For comparison, this table includes the band gaps for some $AZrO_3$ prepared by different methods. All these values are within the range already reported in the literature. The E_g values mainly depend on the preparation methods and experimental conditions like calcinations, purity of the precursor, processing time, etc. These key factors can favor or inhibit the formation of structural defects, which are able to control the degree of structural order and disorder of the material and consequently, the number of intermediary energy levels within the band gap [32]. The slight increase of the band gap of our deposits can be ascribed to the reduction of defects or impurities that give rise to the intermediary energy levels into the band gap of $AZrO_{3-X}$ thin films. Similar phenomena have been observed in the synthesis of other types of perovskites [3,33].

4. Conclusions

$AZrO_{3-X}$ thin films (where A = Ba^{2+}, Ca^{2+} or Sr^{2+}) have been prepared by a photochemical method, followed by post-annealing at 950 °C. The compositional and structural characterization of the samples using XPS and XRD, respectively, revealed the $AZrO_{3-X}$ formation preferably as amorphous structures. The AFM measurements show that samples have a rough and irregular surface, which is characteristic for an amorphous deposit. UV–vis absorption spectra have shown a slight increase of the optical band gap values compared to other deposition methods and this is probably caused by the reduction of intermediary energy levels.

In this study, we have proposed the use of β-diketonate complexes as precursors for the photochemical deposition of ternary metal oxides of perovskite type. In a future work we

Table 2
Data of optical energy band gaps reported in literature for $AZrO_3$ obtained by different methods.

Method employed	Type of $AZrO_3$	Optical gap (eV)	Reference
Photochemical metal organic deposition (PMOD)	$BaZrO_{3-X}$	5.42	This article
Photochemical metal organic deposition (PMOD)	$CaZrO_{3-X}$	5.48	This article
Photochemical metal organic deposition (PMOD)	$SrZrO_{3-X}$	5.33	This article
Hydrothermal microwave method (HMM)	$BaZrO_3$	4.78 and 4.89	[34]
Conventional solid sate reaction (SSR)	$CaZrO_3$	3.93[a] and 5.53[b]	[35]
Polymeric precursor method (PPM)	$SrZrO_3$	4.50–5.21	[36]
Hydrothermal/calcinations method (HCM)	$BaZrO_3$	5.12	[19]
Polymerized complex method (PCM)	$CaZrO_3$	> 4.00	[37]
Sol–gel combustion (SGC)	$SrZrO_3$	5.20	[2]

[a]Theoretical value.
[b]Experimental value.

will apply this proposed photochemical method with single-source precursors. Heterobimetallic complexes, containing all required elements in an already precombined state, may provide a response for the control of stoichiometry and crystallinity of ternary metal oxide films.

Aknowledgements

The authors are grateful to the financial support of National Fund for Scientific and Technological Development, Chile. (FONDECYT no. 1130114). We are also grateful to Professor Markos Maniatis for his valuable suggestions to this manuscript.

References

[1] T.M. Mazzo, M.L. Moreira, I.M. Pinatti, F.C. Picon, E.R. Leite, I.L. V. Rosa, J.A. Varela, L.A. Perazolli, E. Longo, $CaTiO_3$: Eu^{3+} obtained by microwave assisted hydrothermal method: a photoluminescent approach, Opt. Mater. 32 (2010) 990–997.

[2] A. Zhang, M. Lü, S. Wang, G. Zhou, S. Wang, Y. Zhou, Novel photoluminescence of $SrZrO_3$ nanocrystals synthesized through a facile combustion method, J. Alloys Compd. 433 (2007) L7–L11.

[3] L.S. Cavalcante, V.S. Marques, J.C. Sczancoski, M.T. Escote, M.R. Joya, J.A. Varela, M.R.M.C. Santos, P.S. Pizani, E. Longo, Synthesis, structural refinement and optical behavior of $CaTiO_3$powders: a comparative study of processing in different furnaces, Chem. Eng. J. 143 (2008) 299–307.

[4] T. Yu, C.H. Chen, X.F. Chen, W. Zhu, R.G. Krishnan, Fabrication and characterization of perovskite $CaZrO_3$ oxide thin films, Ceram. Int. 30 (2004) 1279–1282.

[5] H. Zhang, X. Fu, S. Niu, Q. Xin, Synthesis and photoluminescence properties of Eu^{3+}-doped $AZrO_3$ (A=Ca, Sr, Ba) perovskite, J. Alloys Compd. 459 (2008) 103–106.

[6] K. Shibuya, T. Ohnishi, M. Kawasaki, H. Koinuma, M. Lippmaa, Growth and structure of wide-gap insulator films on $SrTiO_3$, Solid-State Electron. 47 (2003) 2211–2214.

[7] X. Chen, L. Rieth, M.S. Miller, F. Solzbacher, Pulsed laser deposited Y-doped $BaZrO_3$ thin films for high temperature humidity sensors, Sens. Actuators B 142 (2009) 166–174.

[8] R.B. Mos, M.S. Gabor, M. Nasui, T. Petrisor Jr., C. Badea, A. Rufoloni, L. Ciontea, T. Petrisor, Synthesis of epitaxial $BaZrO_3$ thin films by chemical solution deposition, Thin Solid Films 518 (2010) 4714–4717.

[9] L.S. Cavalcante, A.Z. Simoes, L.P.S. Santos, M.R.M.C. Santos, E. Longo, J.A. Varela, Dielectric properties of $Ca(Zr_{0.05}Ti_{0.95})O_3$ thin films prepared by chemical solution deposition, J. Solid State Chem. 179 (2006) 3739–3743.

[10] M. Andrieux, C. Gasqueres, C. Legros, I. Gallet, M. Herbst-Ghysel, M. Condat, V.G. Kessler, G.A. Seisenbaeva, O. Heintz, S. Poissonnet, Perovskite thin films grown by direct liquid injection MOCVD, Appl. Surf. Sci. 253 (2007) 9091–9098.

[11] R. Pantou, C. Dubourdieu, F. Weiss, J. Kreisel, G. Kobernik, W. Haessler, Effect of substitution of Ti by Zr in $BaTiO_3$ thin films grown by MOCVD, Mater. Sci. Semicond. Process. 5 (2003) 237–241.

[12] B. Marciniak, G.E. Buono-Core, Photochemical properties of 1,3-diketonate transition metal chelates, J. Photochem. Photobiol. A: Chem. 52 (1990) 1–25.

[13] M. Sakamoto, M. Fujistuka, T. Majima, Light as a construction tool of metal nanoparticles: Synthesis and mechanism, J. Photochem. Photobiol. C: Photochem. Rev. 10 (2009) 33–56.

[14] S. Giuffrida, L.L. Costanzo, G.G. Conderelli, G. Ventimiglia, I. L. Fragala, Photochemistry of bis(1,1,1,5,5,5-hexafluoro-2,4-pentanedionato)strontium tetraglyme solutions for eventual liquid phase photochemical deposition, Inorg. Chim. Acta 358 (2005) 1873–1881.

[15] S. Giuffrida, G.G. Conderelli, L.L. Costanzo, G. Ventimiglia, R. Lo Nigro, M. Favazza, E. Votrico, C. Bongiorno, I.L. Fragala, Nickel nanostructured materials from liquid phase photodeposition, J. Nanopart. Res. 4 (2007) 611–619.

[16] G. Cabello, L. Lillo, G.E. Buono-Core, Zr(IV) and Hf(IV) β-diketonate complexes as precursors for the photochemical deposition of ZrO_2 and HfO_2 thin films, J. Non-Cryst. Solids 354 (2008) 982–988.

[17] J.M.A. Nunes, J.W.M. Espinosa, M.F.C. Gurgel, P.S. Pizani, S.H. Leal, M.R.M.C. Santos, E. Longo, Photoluminescent properties of lead zirconate powders obtained by the polymeric precursor method, Ceram. Int. 38 (2012) 4593–4599.

[18] S. Parida, S.K. Rout, L.S. Cavalcante, E. Sinha, M. Siu Li, V. Subramanian, N. Gupta, V.R. Gupta, J.A. Varela, E. Longo, Structural refinement, optical and microwave dielectric properties of $BaZrO_3$, Ceram. Int. 38 (2012) 2129–2138.

[19] V.H. Romero, E. De la Rosa, P. Salas, J.J. Velazquez-Salazar, Strong blue and white photoluminescence emission of $BaZrO_3$ undoped and lanthanide doped phosphor for light emitting diodes application, J. Solid State Chem. 196 (2012) 243–248.

[20] R. Ashiri, A. Nemati, M. Sasani Ghamsari, H. Aadelkhani, Characterization of optical properties of amorphous $BaTiO_3$ nanothin films, J. Non-Cryst. Solids 355 (2009) 2480–2484.

[21] Z.G. Hu, Y.W. Li, M. Zhu, Z.Q. Zhu, J.H. Chu, Microstructural and optical investigations of sol–gel derived ferroelectric $BaTiO_3$ nanocrystalline films determined by spectroscopic ellipsometry, Phys. Lett. A 372 (2008) 4521–4526.

[22] S. Halder, U. Boettger, T. Schneller, R. Waser, O. Baldus, P. Jacobs, M. Wehner, Laser annealing of BST thin films with reduced cracking at an elevated temperature, Mater. Sci. Eng. B 133 (2006) 235–240.

[23] L.L. Jiang, X.G. Tang, S.J. Kuang, H.F. Xiong, Surface chemical states of barium zirconate titanate thin films prepared by chemical solution deposition, Appl. Surf. Sci. 255 (2009) 8913–8916.

[24] R. Koirala, K.R. Gunugunuri, S.E. Pratsinis, P.G. Smirniotis, Effect of zirconia doping on the structure and stability of CaO-based sorbents for CO_2 capture during extended operating cycles, J. Phys. Chem. C 115 (2011) 24804–24812.

[25] C. Tang, X. Lu, F. Huang, M. Cai, Y. Kan, X. Wang, C. Zhang, J. Zhu, Effect of nitrogen doping on optical properties and electronic structures of $SrZrO_3$ films, Solid State Commun. 151 (2011) 280–283.

[26] Z. Xin, Y. Qiuhua, C. Jinjin, XPS study of surface absorbed oxygen of ABO_3 mixed oxides, J. Rare Earths 26 (2008) 511–514.

[27] J.-C. Dupin, D. Gonbeau, P. Vinatier, A. Levasseur, Systematic XPS studies of metal oxides, hydroxides and peroxides, Phys. Chem. Chem. Phys. 2 (2002) 1319–1324.

[28] NIST X-ray Photoelectron Spectroscopy Database 20, Version 4.1 ⟨http://srdata.nist.gov/xps/⟩.

[29] N. Sharma, K.M. Shaju, G.V. Subba Rao, B.V.R. Chowdari, Anodic behaviour and X-ray photoelectron spectroscopy of ternary tin oxides, J. Power Sources 139 (2005) 250–260.

[30] S. Tan, P. Yang, C. Li, W. Wang, J. Wang, M. Zhang, X. Jing, J. Lin, Preparation, characterization and luminescent properties of spherical $CaTiO_3$:Pr^{3+} phosphors by spray pyrolysis, Solid State Sci. 12 (2010) 624–629.

[31] P.V. Nagarkar, P.C. Searson, F.D. Gealy, Effect of surface treatment on $SrTiO_3$: an X-ray photoelectron spectroscopy study, J. Appl. Phys. 69 (1991) 459–462.

[32] M. Shivaram, R.H. Krishna, H. Nagabhushana, S.C. Sharma, B. M. Nagabhushana, B.S. Ravikumar, N. Dhananjaya, C. Shivakumara, J. L. Rao, R.P.S. Chakradhar, Synthesis, characterization, EPR and thermoluminescence properties of $CaTiO_3$ nanophosphor, Mater. Res. Bull. 48 (2013) 1490–1498.

[33] M.D. Goncalves, L.S. Cavalcante, J.C. Scancoski, J.W.M. Espinosa, P. S. Pizani, E. Longo, I.L.V. Rosa, (Sr,Tm)ZrO_3 powders prepared by the polymeric precursor method: synthesis, optical properties and morphological characteristics, Opt. Mater. 31 (2009) 1134–1143.

[34] M.L. Moreira, J. Andres, J.A. Varela, E. Longo, Synthesis of fine micro-sized $BaZrO_3$ powders based on a decaoctahedron shape by the microwave-assisted hydrothermal method, Cryst. Growth Des. 9 (2009) 833–839.

[35] X. Liu, J. Zhang, X. Ma, H. Sheng, P. Feng, L. Shi, R. Hu, Y. Wang, Violet-blue up conversion photostimulated luminescence properties and first principles calculations of a novel un-doped $CaZrO_3$ phosphor for application in optical storage, J. Alloys Compd. 550 (2013) 451–458.

[36] V.M. Longo, L.S. Cavalcante, R. Erlo, V.R. Mastelaro, A.T. de Figueiredo, J.R. Sambrano, S. de Lazaro, A.Z. Freitas, L. Gomez, N. D. Vieira Jr., J.A. Varela, E. Longo, Strong violet-blue light photoluminescence emission at room temperature in $SrZrO_3$: joint experimental and theoretical study, Acta Mater. 56 (2008) 2191–2202.

[37] P. Wu, J. Shi, Z. Zhou, W. Tang, L. Guo, $CaTaO_2N$–$CaZrO_3$ solid solution: band-structure engineering and visible-light-driven photocatalytic hydrogen production, Int. J. Hydrogen Energy 37 (2012) 13704–13710.